



RESEARCH LETTER

10.1002/2015GL065419

Special Section:

First Results from the MAVEN Mission to Mars

Key Points:

- Significant drop in thermospheric temperature between two Martian seasons
- Detection of second layer of OI 297.2 nm emission below 100 km
- Strong correlation between observed mid-UV dayglow and simultaneously measured EUV flux at Mars

Correspondence to:

S. K. Jain,
sonal.jain@lasp.colorado.edu

Citation:

Jain, S. K., et al. (2015), The structure and variability of Mars upper atmosphere as seen in MAVEN/IUVS dayglow observations, *Geophys. Res. Lett.*, 42, 9023–9030, doi:10.1002/2015GL065419.

Received 17 JUL 2015

Accepted 25 SEP 2015

Published online 5 NOV 2015

The structure and variability of Mars upper atmosphere as seen in MAVEN/IUVS dayglow observations

S. K. Jain¹, A. I. F. Stewart¹, N. M. Schneider¹, J. Deighan¹, A. Stiepen¹, J. S. Evans², M. H. Stevens³, M. S. Chaffin¹, M. Crismani¹, W. E. McClintock¹, J. T. Clarke⁴, G. M. Holsclaw¹, D. Y. Lo⁵, F. Lefèvre⁶, F. Montmessin⁶, E. M. B. Thiemann¹, F. Eparvier¹, and B. M. Jakosky¹

¹Laboratory for Atmospheric and Space Physics, University of Colorado Boulder, Boulder, Colorado, USA, ²Computational Physics, Inc., Springfield, Virginia, USA, ³Space Science Division, Naval Research Laboratory, Washington, District of Columbia, USA, ⁴Center for Space Physics, Boston University, Boston, Massachusetts, USA, ⁵Lunar and Planetary Laboratory, University of Arizona, Tucson, Arizona, USA, ⁶LATMOS, CNRS, Guyancourt, France

Abstract We report a comprehensive study of Mars dayglow observations focusing on upper atmospheric structure and seasonal variability. We analyzed 744 vertical brightness profiles comprised of ~109,300 spectra obtained with the Imaging Ultraviolet Spectrograph (IUVS) aboard the Mars Atmosphere and Volatile Evolution (MAVEN) satellite. The dayglow emission spectra show features similar to previous UV measurements at Mars. We find a significant drop in thermospheric scale height and temperature between $L_5 = 218^\circ$ and $L_5 = 337\text{--}352^\circ$, attributed primarily to the decrease in solar activity and increase in heliocentric distance. We report the detection of a second, low-altitude peak in the emission profile of OI 297.2 nm, confirmation of the prediction that the absorption of solar Lyman alpha emission is an important energy source there. The CO_2^+ UV doublet peak intensity is well correlated with simultaneous observations of solar 17–22 nm irradiance at Mars.

1. Introduction

Mars has been studied extensively at ultraviolet wavelengths starting from Mariner 6 and 7 [Barth *et al.*, 1969, 1971; Stewart, 1972; Strickland *et al.*, 1972], Mariner 9 [Stewart *et al.*, 1972, 1973], and more recently by Spectroscopy for Investigation of Characteristics of the Atmosphere of Mars (SPICAM) aboard Mars Express [Bertaux *et al.*, 2006; Leblanc *et al.*, 2006; Simon *et al.*, 2009; Cox *et al.*, 2010; Stiepen *et al.*, 2015]. The results from these measurements reveal a large variability in the composition and structure of the Martian upper atmosphere. However, due to the lack of simultaneous measurements of energy input in the atmosphere, such as solar electromagnetic and particle flux as well as limitations in the observation geometry and data itself, this variability is still not fully understood. The Imaging Ultraviolet Spectrograph (IUVS) is one of the remote sensing instruments on the Mars Atmosphere and Volatile Evolution (MAVEN) spacecraft. MAVEN's observations allows IUVS to conduct limb scans near periapsis, usually at every other orbit, largely without interference from other instruments aboard MAVEN, and can thus observe the Martian atmospheric variability over an extended period with a wide spatial and temporal coverage. The detailed science goals of IUVS are provided by McClintock *et al.* [2014].

In this paper, we present ultraviolet limb scan dayglow observations made by IUVS and study the major characteristic of Martian dayglow and its seasonal variations.

2. Observation Geometry and Data

The MAVEN spacecraft is in an elliptical orbit with apoapsis near 6000 km altitude and periapsis near 160 km [Jakosky *et al.*, 2015]. IUVS carries two detectors: a far ultraviolet (FUV) detector (115–190 nm) and a middle ultraviolet (MUV) detector (180–340 nm) with a spectral resolution of ~0.6 and 1.2 nm, respectively, [McClintock *et al.*, 2014]. The instrument is mounted on an Articulated Payload Platform (APP) that can orient IUVS's field of view relative to Mars depending on spacecraft location, orientation, and desired viewing geometry. IUVS uses a long, narrow slit ($11.3^\circ \times 0.06^\circ$) in the telescope focal plane to provide entrance to

Table 1. Observations of Martian Dayglow From IUVS and Prior Missions

Spacecraft Instrument	L_S (deg)	D_{S-M}^a (AU)	SAZ Range (deg)	$F_{10.7}^b$	T (K) ^c	Peak Brightness (kR)		Peak Altitude (km)	
						CO Cameron	CO ₂ ⁺ UVD ^d	CO Cameron	CO ₂ ⁺ UVD ^e
Mariner 6 ^f	200	1.42	44	180	350	509	–	131	–
Mariner 7 ^g	200	1.42	27	180	350	555	–	129	–
Mariner 9 ^h	312	1.45	7–23	127	325	300	–	138	–
SPICAM ^g	100–130	1.63	30–60	105	200	155	29	118	112.5
SPICAM ^g	138–171	1.52	30–60	105	200	153	30	125	122
IUVS ^h	218	1.4	30–72	160	300	583	76	127.5	127.5
IUVS ^h	337–352	1.5	10–73	110	250	440	56	122.5	122.5

^aSun-Mars distance.

^b $F_{10.7}$ is the solar EUV flux index (in units of 10^{-22} W/m²/Hz), measured at 1 AU, and corrected for Sun-Earth-Mars angle.

^cTemperature values retrieved from CO₂⁺ UVD profile. References are same as provided for instrument.

^dStudies on Mariner 6, 7, and Mariner 9 did not report CO₂⁺ UVD brightness near the airglow peak.

^eBarth *et al.* [1971] and Stewart [1972].

^fStewart *et al.* [1972].

^gLeblanc *et al.* [2006]; values are for SAZ = 15–37°.

^hValues are for SAZ = 30–45°.

the spectrograph, which defines the instrument instantaneous field of view. Limb-scanning observations are made when the spacecraft is close to the planet (below 500 km). The APP orients IUVS’s line of sight perpendicular to spacecraft motion, and the projection of slit onto the atmosphere is perpendicular to the planet’s radius vector at slit center (parallel to the tangent vector at slit center). During near beginning and end of a periape pass, the slit can be tilted up to 13° with respect to the horizon [McClintock *et al.*, 2014]. The APP and scan mirror motion allow IUVS to repeatedly map out the vertical structure of the atmosphere between 80 and 250 km with a vertical resolution of ~5 km, while the spacecraft travels through ~90° of true anomaly [McClintock *et al.*, 2014; Schneider *et al.*, 2015]. Each periape orbit phase spans ~22 min and consists of 12 scans. In this mode, IUVS slit is divided into seven bins along the slit, which along with scan mirror motion provides seven altitude profiles per scan. These seven profiles are sorted by altitude (5 km resolution) and combined into a single profile in the present analysis (12 profiles/periape).

We have divided the data set into two solar longitude sets $L_S \sim 218^\circ$ (18–22 October 2014) and $L_S = 337–352^\circ$ (5 May to 2 June 2015). For $L_S \sim 218^\circ$, our analysis includes 19 orbits (109–128) except for orbit 115, when the spacecraft was in safe mode during the maximum predicted dust fluence associated with the comet C/2013 A1 Siding Spring’s close flyby of Mars [Schneider *et al.*, 2015, and references therein]. For L_S between 337° and 352°, 43 orbits are used; every other orbit between 1160 and 1220, and between 1275 and 1309 (except orbits 1198, 1216, 1289, and 1295). A total of 109,368 individual spectra are used to generate 744 altitude profiles (228 for $L_S = 218^\circ$ and 516 for $L_S = 337–352^\circ$). The occasional gaps in between the nominal periape observation mode are due to sharing pointing control with other instruments, communication passes, solar Keep-Out Zone constraints, calibration activities, and other irregularities. The lighting and geometry for the IUVS observations are given in Table 1.

Figure 1 shows the color composite of MUV and FUV detectors assembled from a full limb scan (orbit 110) of the Martian airglow layer. In the MUV channel, the CO Cameron ($a^3\Pi - X^1\Sigma^+$) band system between 175 and 270 nm, CO₂⁺ ultraviolet doublet (UVD, $B^2\Sigma^+ - X^2\Pi_g$) near 289 nm, CO₂⁺ Fox-Duffendack-Barker (FDB, $A^2\Pi_u - X^2\Pi_g$) bands near 310–330 nm, and OI ($^3P - ^1S$) 297.2 nm emissions are prominent as expected from previous observations by Mariner 6 and 7 [Barth *et al.*, 1971], Mariner 9 [Stewart *et al.*, 1972], and SPICAM/Mars Express [Leblanc *et al.*, 2006]. The prominent features in FUV consist of H Ly α , OI 130.4 and 135.6 nm, Cl 156.1 and 165.7 nm, ClII 133.5 nm, and CO fourth positive ($A^1\Pi - X^1\Sigma^+$) band system. Figure 1 (bottom) shows the averaged spectra in the FUV and MUV observed at altitudes between 120 and 130 km.

IUVS has also detected N₂ Vegard-Kaplan bands in the MUV and for the first time, the N₂ Lyman-Birge-Hopfield bands in Mars’s FUV dayglow; details are reported in Stevens *et al.* [2015].

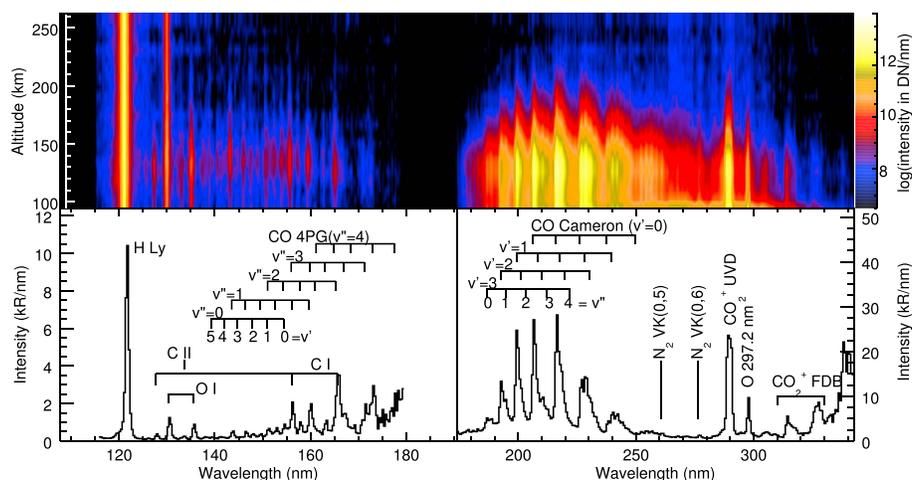


Figure 1. (top) The IUVS's FUV and MUV detectors color composite generated using a full vertical scan from orbit 110 (2059 UTC, 18 October 2014), one of the 744 profiles. The horizontal and vertical axes represent wavelength and altitude (80–250 km), respectively. (bottom) Calibrated FUV and MUV spectra obtained from the same scan; these are averages of 13 individual spectra obtained between 120 and 135 km.

3. Analysis of IUVS Data and Results

As shown in Figure 1, the Martian ultraviolet dayglow spectrum is a blended composite of many emission features, each of which is identified from its expected location and shape in the spectrum. We have used a multiple linear regression (MLR) method to fit the observed spectrum. Aside from atomic and molecular emissions described above, the fit templates include a reference-reflected solar spectrum measured by IUVS during disk observations. The inclusion of this spectrum is important at altitudes below 100 km, where solar scattered light can appear in the MUV spectra both from high-altitude clouds and dust, and from stray light within the instrument. Other templates use the IUVS line spread function (LSF), obtained from an IUVS observation of interplanetary and Mars coronal hydrogen Lyman- α . More details about MLR, the LSF, and the synthetic spectrum are given in *Stevens et al.* [2015] and *Evans et al.* [2015].

The observed raw data numbers (DN) are corrected for detector dark current and then converted to physical brightness in Rayleigh using the sensitivity derived from UV bright stellar observations made during the MAVEN cruise phase [*McClintock et al.*, 2014]. The MUV and FUV systematic uncertainty estimated from these stellar calibrations are $\pm 30\%$ and $\pm 25\%$, respectively. The flatfield errors have not been corrected in the data, which can introduce additional 10% uncertainty. A detailed study on IUVS calibrations and instrument performance is currently underway.

3.1. Altitude Profiles of Thermospheric Emission

To derive the brightness of the emissions, the fitted spectra of targeted emissions from each section of the slit are binned at 5 km altitude intervals. Figure 2 shows the altitude profiles of CO Cameron, CO_2^+ UVD, OI 297.2 nm, and CO_2^+ FDB bands, for the two seasons and solar zenith angles 30–45° (top) and 50–70° (bottom).

Some of the spectra used in this analysis (for $L_S = 345^\circ$) captured only wavelength ≥ 198 nm (affects total CO Cameron band intensity). Comparison with the complete spectra shown that these contained 83% of the total CO Cameron band intensity. A normalization factor of 1.21 has therefore been applied to CO Cameron band intensity observed during $L_S = 345^\circ$.

The peak intensities of the CO_2^+ UVD and CO Cameron bands are about 35% higher for $L_S = 218^\circ$ than for $L_S \sim 345^\circ$. This difference is readily accounted for by changes in heliocentric distance and solar activity (see Table 1). As expected from Chapman theory, we find that the variation of peak intensities of CO Cameron band and CO_2^+ doublet emission vary as the cosine of solar zenith angle (SZA) [*Schunk and Nagy*, 2000]. The altitude of the maximum dayglow intensity is ~ 127 km and 122 km (for CO Cameron and CO_2^+ UVD) for $L_S = 218^\circ$ and $L_S \sim 345^\circ$, respectively. Large dust storms on Mars also affect the peak altitude [*Stewart et al.*, 1972; *Leblanc et al.*, 2006]. There was regional dust storm activity near $L_S \sim 217$, but it was minor compared to the storms of 1971 and 2007 (S. W. Bougher, personal communication, 2015). We did not find any signifi-

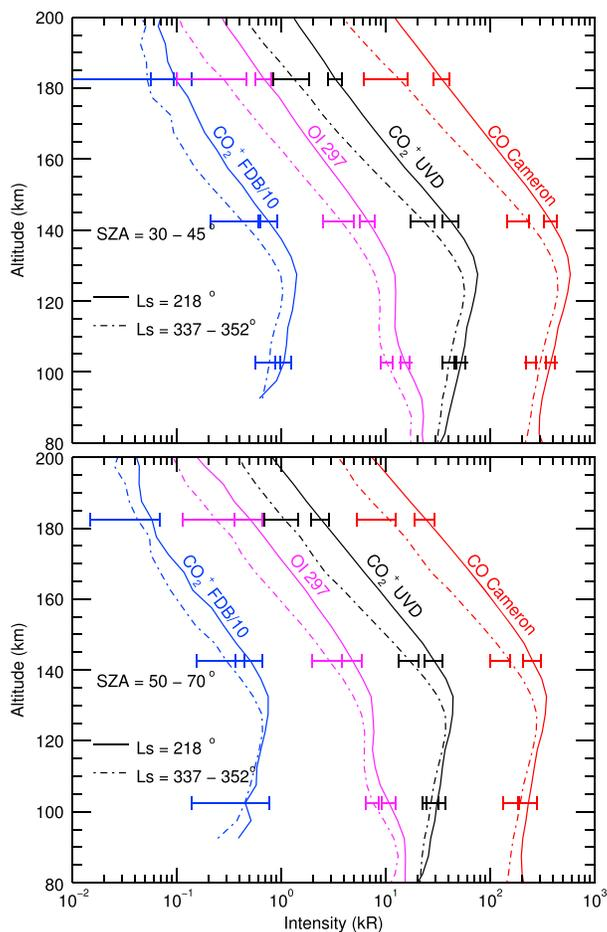


Figure 2. Mean altitude profiles for the CO_2^+ ultraviolet doublet, CO Cameron band, OI 297.2 nm, and CO_2^+ Fox-Duffendack-Barker bands for two solar longitudes and (top) SZA = 30–45° and (bottom) SZA = 50–70°. Solid curves show the brightness for $L_S = 218^\circ$, and dash-dotted curves shows them for $L_S \sim 345^\circ$. The intensity of CO_2^+ FDB band is divided by a factor of 10. Horizontal bars show the standard deviation of the profiles. The intensities decrease by $\sim 50\%$ for SZA = 50–70°.

cant dependence of the peak altitude on SZA. For the present observations, SZAs are highly correlated with latitude. The Chapman theory for a given temperature profile predicts increase in peak altitude for higher SZA, but this might be offset by a decrease in lower thermospheric temperature at higher latitudes and for SZAs.

Compared to the SPICAM observations, the maximum intensities of CO Cameron band and CO_2^+ UVD observed by IUVS is ~ 3 times higher. Most of the differences in the intensity are due to solar activity and Sun-Mars distance (see Table 1). IUVS observations conditions are more similar to Mariner 6, 7, and 9 than SPICAM because they were taken near perihelion and during moderate to high solar activity period. Nonetheless, the overall variation in Martian dayglow is not fully understood.

Figure 2 presents CO_2^+ FDB and OI 297 nm emission profiles. At Mars, the major CO_2^+ FDB excitation sources include photoionization of CO_2 and solar fluorescent scattering from CO_2^+ . Fluorescent scattering becomes the dominant source at higher altitudes (> 160 km), which accounts for the increase in their scale height at higher altitudes [Fox and Dalgarno, 1979; Fox, 1992]. These bands may be used to infer the ion densities of CO_2^+ [Evans et al., 2015].

The OI 297.2 nm emission originates from the $\text{O}(^1\text{S} \rightarrow ^3\text{P})$ transition. This emission has been observed by Mariner 6 and 7 [Stewart, 1972] and SPICAM [Gronoff et al., 2012]. The major production source of $\text{O}(^1\text{S})$ in the Martian atmosphere is photodissociation of CO_2 [Fox and Dalgarno, 1979; Gronoff et al., 2012; Bhardwaj and Jain, 2013], and its production rate has two distinct peaks: one below 100 km due to solar

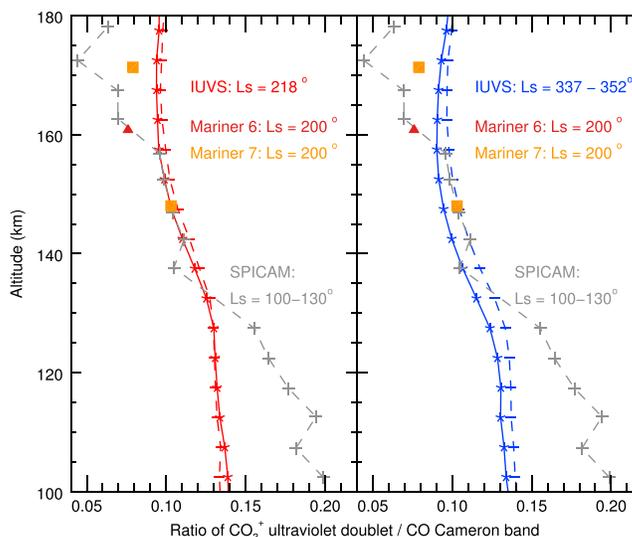


Figure 3. Ratio of Cameron band and CO_2^+ UVD for (left) $L_S = 218^\circ$ and (right) $L_S \sim 345^\circ$ seasons and $\text{SZA} = 30\text{--}45^\circ$ (solid curves) and $50\text{--}70^\circ$ (dashed curve). Gray dashed curves: intensity ratio taken for SPICAM measurements carried out at $L_S = 100\text{--}130^\circ$ and $\text{SZA} = 15\text{--}37^\circ$ [Leblanc *et al.*, 2006]. Triangle: intensity ratio deduced by Leblanc *et al.* [2006] for Mariner 6 at $\text{SZA} = 27^\circ$ and $L_S = 200^\circ$. Squares: intensity ratio deduced by Leblanc *et al.* [2006] for Mariner 7 at $\text{SZA} = 44^\circ$ and $L_S = 200^\circ$.

Lyman α and another peak at 120–130 km due to EUV absorption [Fox and Dalgarno, 1979; Simon *et al.*, 2009; Gronoff *et al.*, 2012; Bhardwaj and Jain, 2013]. None of the previous observations reported a lower peak of OI 297.2 nm, because of scattered solar light below 100 km. Due to low amount of stray light in the IUVS data, we have fitted and removed the solar continuum from the periapse data below 100 km and find evidence of a second peak in the OI 297.2 nm brightness profile. The detection of lower peak of OI 297.2 nm emission is important in light of simultaneous observations of solar Lyman alpha irradiance by extreme ultraviolet monitor (EUVM)/MAVEN. This will enable us to constrain the yield of $\text{O}(^1\text{S})$ atoms in photodissociation of CO_2 at 121.6 nm wavelength [Fox and Dalgarno, 1979; Gronoff *et al.*, 2012; Bhardwaj and Jain, 2013]. A clear IUVS detection of OI 297.2 nm emission lower peak might also help understand/reinterpret SPICAM observation of OI 297.2 nm brightness below 100 km.

The upper peak intensity of OI 297.2 nm (for $\text{SZA} = 30\text{--}45^\circ$) is ~ 12 kR (8 kR) for $L_S = 218^\circ$ ($L_S \sim 345^\circ$). Stewart [1972] reported a value of ~ 20 kR at 120 km, whereas Gronoff *et al.* [2012] reported a value of 4.5 kR ($\text{SZA} = 40^\circ$, $F_{10.7} = 115$, $L_S = 148^\circ$) near 125 km (G. Gronoff, personal communication, 2014). The upper peak intensity of OI 297 nm emission observed by Mariner and IUVS agree but are about a factor 4 higher than that reported by Gronoff *et al.* [2012]. This difference can partly be explained due to solar activity and the heliocentric distance of Mars between IUVS and Mariner, and SPICAM observations.

Figure 3 shows the ratio of CO_2^+ UVD to the CO Cameron band. The ratio is ~ 0.14 below 135 km and ~ 0.10 above 160 km. The ratio decreases rapidly between 135 and 160 km, and it shows that the CO Cameron band brightness does not arise solely from dissociative excitation of CO_2 , and contributions from dissociative recombination of CO_2^+ and electron impact on CO become important at higher altitudes [Fox and Dalgarno, 1979; Jain and Bhardwaj, 2012; Stiepen *et al.*, 2015]. The ratio does not change significantly with the SZA .

A detailed model calculation for IUVS dayglow data is underway to quantify the role of various production sources of $\text{CO}(a^3\Pi)$ and $\text{CO}_2^+(B^2\Sigma_u^+)$.

3.2. Scale Height and Temperature

The primary sources of both $\text{CO}(a^3\Pi)$ and $\text{CO}_2^+(B^2\Sigma_u^+)$ involve dissociation/ionization of CO_2 , making them a useful tool to infer the neutral atmosphere scale height. As discussed in the previous section, the ratio of CO_2^+ doublet to CO Cameron band does not vary significantly between 150 and 180 km; thus, we have chosen this region of atmosphere to derive the scale heights from CO Cameron band and CO_2^+ doublet emission

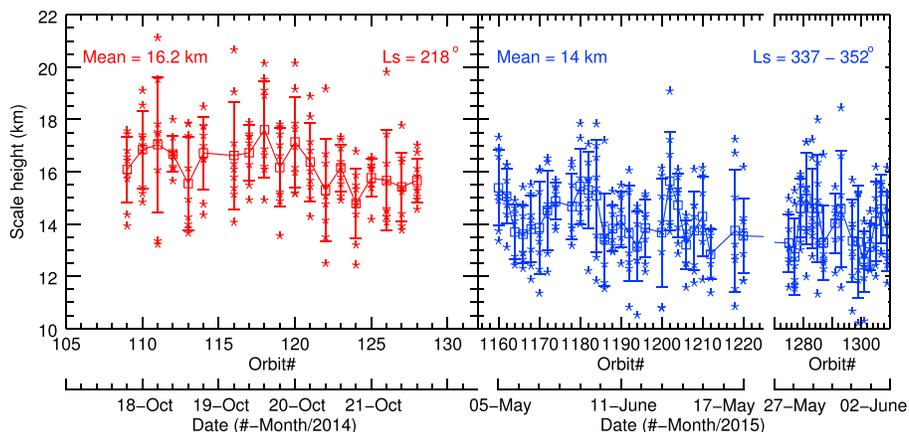


Figure 4. Variation of CO_2^+ ultraviolet doublet scale height for two seasons. Symbol shows the derived scale height for each individual scan in an orbit. Thick colored lines show the mean scale height and thin lines show the standard deviation for each orbit. The mean scale height for $L_S = 218^\circ$ and $L_S \sim 345^\circ$ are 16.2 ± 0.12 km and 14 ± 0.1 km, respectively. The error on scale height determination is smaller than the observed variations within an orbit.

profiles assuming an isothermal atmosphere. The scale height is calculated by fitting an exponential function to topside portion of brightness profile using a Levenber-Marquardt least squares minimization algorithm.

Figure 4 shows the scale height derived from CO_2^+ doublet emission. The scale heights derived from our measurements show statistically significant variations even within an orbit. The minimum and maximum values of scale heights derived for $L_S = 218^\circ$ ($L_S = 337-352^\circ$) are 12.7 km (10.2 km) and 21 km (18.5 km), respectively. Such variability in scale heights was also reported by *Stewart et al.* [1972] for Mariner 9 and by *Leblanc et al.* [2006] and *Stiepen et al.* [2015] for SPICAM data. This large variability in scale height might be due to strong coupling between the lower and upper atmosphere via wave and tidal activities [*Stewart et al.*, 1972; *Bougher et al.*, 2001; *Forbes et al.*, 2008; *Stiepen et al.*, 2015]. A study on atmospheric tides in Martian atmosphere using IUVS dayglow data is presented by *Lo et al.* [2015].

The mean scale height for the two seasons is 16.2 ± 0.1 km and 14 ± 0.1 km with a standard deviation of 1.6 km for both seasons. The uncertainty in scale height is dominated by intrinsic variability as opposed to measured error. These scale heights correspond to a mean thermospheric temperature of 300 ± 2 K and 250.6 ± 1.7 K for $L_S = 218^\circ$ and $L_S = 337-352^\circ$, respectively, (standard deviation is 29 K for both seasons). This indicates ~ 50 K cooling over this time period, consistent with the altitude profile shapes presented in Figure 2. *Evans et al.* [2015] have used the CO_2^+ UVD profiles to retrieve the density of CO_2 . They also inferred the temperature from retrieved CO_2 densities between 150 and 220 km and reported a mean temperature of 325 ± 25 K for $L_S = 218^\circ$. Their calculated temperature is about 25 K higher than that in our study for the same period. The difference in temperature could be due to their choice of altitude region to infer the temperature, uncertainty in the retrieved density, and quality of fit.

We did not find any significant dependence of scale height on the latitude or solar zenith angle, which is consistent with the studies of *Stewart et al.* [1972], *Leblanc et al.* [2006], and *Stiepen et al.* [2015]. *Leblanc et al.* [2006] reported a mean scale height of ~ 11.2 km and ~ 14 km derived from CO_2^+ doublet and CO Cameron bands, respectively, which resulted in a temperature difference of ~ 50 K estimated from the two emission profiles. The mean scale height derived from CO Cameron profiles in our study is 16.7 ± 0.1 km (13.9 ± 0.1 km) for $L_S = 218^\circ$ ($L_S = 337-352^\circ$), consistent with the scale height derived from CO_2^+ doublet emission. *Stiepen et al.* [2015] have also not found any statistical difference between the scale heights derived from the CO Cameron band and CO_2^+ UVD emissions.

3.3. Effects of Solar EUV Flux

Figure 5 (top) shows the short-term variation of maximum intensity of CO_2^+ doublet ($L_S = 337-352^\circ$ and $\text{SZA} = 30-40^\circ$) with respect to the orbital average extreme ultraviolet channel irradiance (17–22 nm: solar irradiance mainly responsible for photoionization) of the extreme ultraviolet monitor (EUVM) on board MAVEN [*Eparvier et al.*, 2015]. There is a positive correlation between peak intensities of CO_2^+ doublet bands

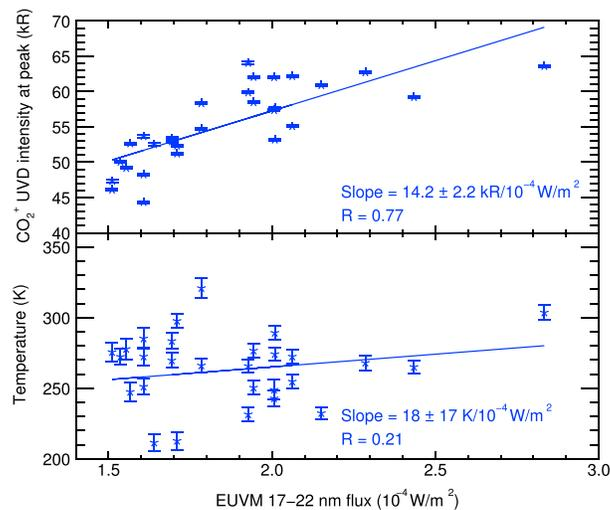


Figure 5. Short-term variations of (top) CO_2^+ doublet maximum intensity and (bottom) topside temperature with 17–22 nm irradiance measured by the EUVM instrument aboard MAVEN. Values are for $L_S \sim 337\text{--}343^\circ$ (orbits 1160–1220) and SZA between 30° and 40° . R is the linear correlation coefficient.

(Figure 5, top) and CO Cameron (not shown) and the EUV flux. Although this is expected, such simultaneous observations of the dayglow and the local solar forcing have heretofore not been made. *Stewart et al.* [1972] reported a dependence of CO Cameron band peak intensity with $F_{10.7}$, measured at Earth and corrected for Mars–Earth–Sun angle.

Figure 5 (bottom) shows the short-term variation of derived temperature with 17–22 nm irradiance for $L_S \sim 345^\circ$ and SZA = $30\text{--}45^\circ$. The temperatures show a little to no dependence on EUV flux (the slope is statistically insignificant). *Stewart et al.* [1972] also did not find any correlation between scale height and $F_{10.7}$ flux. The lack of correlation between solar EUV flux and temperature for small subset of data (5–18 May 2015) suggests that on short timescales, the temperature variability in the upper atmosphere depends not so much on solar activity but rather on wave and/or tidal activity from lower atmosphere [*Stewart et al.*, 1972; *Stiepen et al.*, 2015]. However, on longer timescales when changes in the solar EUV flux becomes dominant, the mean temperature in the upper atmosphere does respond to solar EUV flux as shown in temperature difference between the two seasons. *Forbes et al.* [2006] also found the response of Mars thermosphere to the quasiperiodic (27 day) variation of solar flux. In the future, we will use large IUVS dayglow data sets to study the overall impact of solar EUV flux on thermospheric temperatures. This also underscores the need for monitoring the EUV solar flux at Mars when assessing the Martian upper atmosphere response to solar forcing.

4. Conclusions

We report early IUVS/MAVEN observations of Martian UV dayglow spanning two seasons $L_S = 218^\circ$ (18–22 October 2014) and $L_S = 337\text{--}352^\circ$ (5 May to 2 June 2015). The altitude profiles for major atmospheric emissions have been generated by binning the spectra in altitude. The average peak emission intensity and peak altitude have decreased by about 30% and ~ 5 km, respectively, between October 2014 and May 2015, which corresponds to a decrease in solar activity and an increase in heliocentric distance between the two seasons. We report the first indication of a lower peak (below 100 km) in OI 297.2 nm emission; this lower peak is produced solely by photodissociation of CO_2 by solar Lyman alpha.

We have retrieved the scale height and thermospheric temperatures from dayglow altitude profiles, which shows large variability even within an orbit, consistent with earlier findings [*Stewart et al.*, 1972; *Leblanc et al.*, 2006; *Stiepen et al.*, 2015], indicating a strong coupling between lower and upper Martian atmosphere. The temperatures derived for IUVS measurements for $L_S = 218^\circ$ and $L_S \sim 345^\circ$ are 300 ± 2 K and 250 ± 1.7 K. We observed a positive linear correlation between the CO_2^+ UVD and CO Cameron bands peak intensity and simultaneous measured solar 17–22 nm irradiance by the EUV monitor aboard MAVEN. We noticed that solar

forcing is not a very important factor in determining upper atmosphere temperatures for short timescales, but it does affect the mean upper atmosphere temperature over long timescales. This simultaneous monitoring of both the UV dayglow and the local EUV flux represents a significant advance in understanding how planetary atmospheres respond to solar forcing.

Acknowledgments

The MAVEN project is supported by NASA through the Mars Exploration Program. The data used (tagged "periapse" with version/revision tag v03_r01) are archived in NASA's Planetary Data System (PDS). D. Lo is supported by the MAVEN project through a subcontract to the University of Arizona (NASA grant NNN10CCO4C). M.H. Stevens is supported by the NASA MAVEN Participating Scientist Program. A. Stiepen is supported by the Belgian American Educational Foundation and the Rotary District 1630.

References

- Barth, C. A., W. G. Fastie, C. W. Hord, J. B. Pearce, K. K. Kelly, A. I. Stewart, G. E. Thomas, G. P. Anderson, and O. F. Raper (1969), Mariner 6 and 7: Ultraviolet spectrum of Mars upper atmosphere, *Science*, *165*, 1004–1005.
- Barth, C. A., C. W. Hord, J. B. Pearce, K. K. Kelly, G. P. Anderson, and A. I. Stewart (1971), Mariner 6 and 7 ultraviolet spectrometer experiment: Upper atmosphere data, *J. Geophys. Res.*, *76*, 2213–2227, doi:10.1029/JA076i010p02213.
- Bertaux, J.-L., et al. (2006), SPICAM on Mars Express: Observing modes and overview of UV spectrometer data and scientific results, *J. Geophys. Res.*, *111*, E10590, doi:10.1029/2006JE002690.
- Bhardwaj, A., and S. K. Jain (2013), CO Cameron band and CO₂⁺ UV doublet emissions in the dayglow of Venus: Role of CO in the Cameron band production, *J. Geophys. Res. Space Physics*, *118*, 3660–3671, doi:10.1002/jgra.50345.
- Bougher, S. W., S. Engel, D. P. Hinson, and J. M. Forbes (2001), Mars Global Surveyor Radio Science electron density profiles: Neutral atmosphere implications, *Geophys. Res. Lett.*, *28*, 3091–3094.
- Cox, C., J. C. Gérard, B. Hubert, J. L. Bertaux, and S. W. Bougher (2010), Mars ultraviolet dayglow variability: SPICAM observations and comparison with airglow model, *J. Geophys. Res.*, *115*, E04010, doi:10.1029/2009JE003504.
- Eparvier, F. G., P. C. Chamberlin, T. N. Woods, and E. M. B. Thiemann (2015), The solar extreme ultraviolet monitor for MAVEN, *Space Sci. Rev.*, *1–9*, doi:10.1007/s11214-015-0195-2.
- Evans, J. S., et al. (2015), Retrieval of CO₂ and N₂ in the Martian thermosphere using dayglow observations by IUUVS on MAVEN, *Geophys. Res. Lett.*, *42*, doi:10.1002/2015GL065489.
- Forbes, J. M., S. Bruinsma, and F. G. Lemoine (2006), Solar rotation effects on the thermospheres of Mars and Earth, *Science*, *312*(5778), 1366–1368, doi:10.1126/science.1126389.
- Forbes, J. M., F. G. Lemoine, S. L. Bruinsma, M. D. Smith, and X. Zhang (2008), Solar flux variability of Mars' exosphere densities and temperatures, *Geophys. Res. Lett.*, *35*, L01201, doi:10.1029/2007GL031904.
- Fox, J. L. (1992), Airglow and aurora in the atmospheres of Venus and Mars, in *Venus and Mars: Atmospheres, Ionospheres, and Solar Wind Interactions*, *Geophys. Monogr. Ser.*, vol. 66, edited by J. G. Luhmann, M. Tatallyay, and R. O. Pepin, pp. 191–222, AGU, Washington, D. C.
- Fox, J. L., and A. Dalgarno (1979), Ionization, luminosity, and heating of the upper atmosphere of Mars, *J. Geophys. Res.*, *84*, 7315–7333, doi:10.1029/JA084iA12p07315.
- Gronoff, G., C. S. Wedlund, C. J. Mertens, M. Barthélemy, R. J. Lillis, and O. Witasse (2012), Computing uncertainties in ionosphere-airglow models. II—The Martian airglow, *J. Geophys. Res.*, *117*, A05309, doi:10.1029/2011JA017308.
- Jain, S. K., and A. Bhardwaj (2012), Impact of solar EUV flux on CO Cameron band and CO₂⁺ UV doublet emissions in the dayglow of Mars, *Planet. Space Sci.*, *63–64*, 110–122, doi:10.1016/j.pss.2011.08.010.
- Jakosky, B. M., et al. (2015), The Mars Atmosphere and Volatile Evolution (MAVEN) mission, *Space Sci. Rev.*, *1–46*, doi:10.1007/s11214-015-0139-x.
- Leblanc, F., J. Y. Chaufray, J. Lilensten, O. Witasse, and J.-L. Bertaux (2006), Martian dayglow as seen by the SPICAM UV spectrograph on Mars Express, *J. Geophys. Res.*, *111*, E09511, doi:10.1029/2005JE002664.
- Lo, D. Y., et al. (2015), Non-migrating tides in the Martian atmosphere as observed by MAVEN IUUVS, *Geophys. Res. Lett.*, *42*, doi:10.1002/2015GL066268.
- McClintock, W. E., N. M. Schneider, G. M. Holsclaw, J. T. Clarke, A. C. Hoskins, I. Stewart, F. Montmessin, R. V. Yelle, and J. Deighan (2014), The Imaging Ultraviolet Spectrograph (IUUVS) for the MAVEN mission, *Space Sci. Rev.*, *1–50*, doi:10.1007/s11214-014-0098-7.
- Schneider, N. M., et al. (2015), MAVEN IUUVS observations of the aftermath of the comet siding spring meteor shower, *Geophys. Res. Lett.*, *42*, 4755–4761, doi:10.1002/2015GL063863.
- Schunk, R. W., and A. F. Nagy (2000), Ionospheres: Physics, plasma physics, and chemistry.
- Simon, C., O. Witasse, F. Leblanc, G. Gronoff, and J.-L. Bertaux (2009), Dayglow on Mars: Kinetic modeling with SPICAM UV limb data, *Planet. Space Sci.*, *57*, 1008–1021, doi:10.1016/j.pss.2008.08.012.
- Stevens, M. H., et al. (2015), New observations of molecular nitrogen in the Martian upper atmosphere by IUUVS on MAVEN, *Geophys. Res. Lett.*, *42*, doi:10.1002/2015GL065319.
- Stewart, A. I. (1972), Mariner 6 and 7 ultraviolet spectrometer experiment: Implication of CO₂⁺, CO, and O airglow, *J. Geophys. Res.*, *77*, 54–68, doi:10.1029/JA077i001p00054.
- Stewart, A. I., C. A. Barth, C. W. Hord, and A. L. Lane (1972), Mariner 9 ultraviolet spectrometer experiment: Structure of Mars' upper atmosphere, *Icarus*, *17*(2), 469–474, doi:10.1016/0019-1035(72)90012-7.
- Stiepen, A., J.-C. Gérard, S. Bougher, F. Montmessin, B. Hubert, and J.-L. Bertaux (2015), Mars thermospheric scale height: CO Cameron and CO₂⁺ dayglow observations from Mars Express, *Icarus*, *245*, 295–305, doi:10.1016/j.icarus.2014.09.051.
- Strickland, D. J., G. E. Thomas, and P. R. Sparks (1972), Mariner 6 and 7 ultraviolet spectrometer experiment: Analysis of the OI 1304 and 1356 Å emissions, *J. Geophys. Res.*, *77*, 4052–4068, doi:10.1029/JA077i022p04052.
- Strickland, D. J., A. I. Stewart, C. A. Barth, C. W. Hord, and A. L. Lane (1973), Mariner 9 ultraviolet spectrometer experiment: Mars atomic oxygen 1304 Å emission, *J. Geophys. Res.*, *78*, 4547–4559, doi:10.1029/JA078i022p04547.